Microscopy and Microanalysis, 2024, **30**, 1057–1065
https://doi.org/10.1093/mam/ozae035
Advance access publication 20 May 2024
Original Article

Microscopy AND Microanalysis

Facilitating Atom Probe Tomography of 2D MXene Films by In Situ Sputtering

Mathias Krämer[1,*], Bar Favelukis[2], Maxim Sokol[2], Brian A. Rosen[2], Noam Eliaz[2], Se-Ho Kim[1,3], and Baptiste Gault[1,4,*]

[1]*Max Planck Institute for Sustainable Materials, Max-Planck-Straße 1, Düsseldorf 40237, Germany*
[2]*Department of Materials Science and Engineering, Tel Aviv University, P.O.B 39040, Ramat Aviv 6997801, Israel*
[3]*Department of Materials Science and Engineering, Korea University, Seoul 02841, Republic of Korea*
[4]*Department of Materials, Royal School of Mines, Imperial College London, London SW7 2AZ, UK*

***Corresponding authors:** Mathias Krämer, E-mail: m.kraemer@mpie.de; Baptiste Gault, Email: b.gault@mpie.de

Abstract

2D materials are emerging as promising nanomaterials for applications in energy storage and catalysis. In the wet chemical synthesis of MXenes, these 2D transition metal carbides and nitrides are terminated with a variety of functional groups, and cations such as Li^+ are often used to intercalate into the structure to obtain exfoliated nanosheets. Given the various elements involved in their synthesis, it is crucial to determine the detailed chemical composition of the final product, in order to better assess and understand the relationships between composition and properties of these materials. To facilitate atom probe tomography analysis of these materials, a revised specimen preparation method is presented in this study. A colloidal $Ti_3C_2T_z$ MXene solution was processed into an additive-free free-standing film and specimens were prepared using a dual beam scanning electron microscope/focused ion beam. To mechanically stabilize the fragile specimens, they were coated using an *in situ* sputtering technique. As various 2D material inks can be processed into such free-standing films, the presented approach is pivotal for enabling atom probe analysis of other 2D materials.

Key words: 2D materials, atom probe tomography, focused ion beam, *in situ* coating, MXenes

Introduction

Since the groundbreaking experimental observation of graphene (Novoselov et al., 2004), there has been significant interest in 2D materials and their fascinating functional properties. Following graphene, the successful synthesis of other 2D elemental materials (Mannix et al., 2017), 2D transition metal dichalcogenides (Manzeli et al., 2017) and 2D perovskites (Lan et al., 2019), to name a few, has significantly expanded the landscape of 2D materials. Because 2D materials have a thickness of one up to a few atomic layers, and thus a high surface-to-volume ratio, they are particularly interesting for applications involving highly surface-active chemical processes, such as energy storage or catalysis (Nicolosi et al., 2013).

MXenes, 2D transition metal carbides and nitrides, have also been the subject of intense research since their discovery by the Barsoum and Gogotsi groups (Naguib et al., 2011). To date, more than 50 different compositions have been synthesized, not even considering the different and highly variable surface chemistries (VahidMohammadi et al., 2021; Anasori et al., 2023). Their top-down synthesis involves two steps, namely the harsh selective etching of the A layer (typically Al, Si, or Ga) from a bulk MAX phase(-like) precursor in a typically HF-based wet chemical environment, and the subsequent exfoliation of the obtained weakly bonded multilayer MXenes into individual nanosheets by intercalation of cations or molecules (Alhabeb et al., 2017; Lim et al., 2022). The general chemical formula of MXenes is written as $M_{n+1}X_nT_z$, characterized by $n + 1$ atomic layers of one or more early transition metals M and n interleaved atomic layers of C and/or N, denoted as X, where T_z represents surface termination groups saturating the bare surface during synthesis. Because this synthesis process is scalable (Shuck et al., 2020), and the MXene nanosheets can be easily processed into free-standing films (Zhang et al., 2020) or printable inks (Zhang et al., 2019), they are attractive and accessible for industrial applications.

The resulting properties are significantly influenced by the detailed synthesis parameters (Thakur et al., 2023), which control in particular the flake size, defect density, and surface chemistry. A carefully optimized synthesis route can therefore be used to fine-tune the properties of the MXenes, which is comparable to defect engineering in bulk materials (Li & Lu, 2017). However, Shuck pointed out that MXenes are unfortunately often treated as chemicals rather than materials, because the detailed synthesis route is overlooked (Shuck, 2023). For example, in many synthesis protocols for $Ti_3C_2T_z$, the most studied MXene to date, spontaneous intercalation of Li cations (Lukatskaya et al., 2013) is crucial for obtaining large and high quality, i.e. less defective, monolayer MXene flakes (Ghidiu et al., 2014; Lipatov et al., 2016; Sang et al., 2016; Shekhirev et al., 2022). Although it is known that the presence of Li influences the properties of the MXenes (Chen et al., 2020), it remains a difficult task to localize and quantify Li in the material using the commonly applied techniques (Shekhirev et al., 2021).

Received: November 30, 2023. **Revised:** February 16, 2024. **Accepted:** March 31, 2024

Atom probe tomography (APT) is an analytical characterization technique with sensitivity to both light and heavy elements and sufficient spatial resolution to address these unanswered questions (Gault et al., 2021). Briefly summarized, the atom probe is a time-of-flight mass spectrometer equipped with a position-sensitive detector, where individual atomic or molecular ions are field evaporated from the apex of a sharp, needle-shaped specimen. In combination, the recorded time-of-flight and the impact coordinates of the ions on the detector, allow compositional mapping with a sub-nanometer spatial resolution in 3D (De Geuser & Gault, 2020). Given these capabilities, APT has been increasingly used in recent years to characterize functional nanomaterials, such as nanoparticles for catalysis, as it provides unique compositional insights that enable an understanding of the activity and degradation of these materials (Li et al., 2022).

A critical step towards the APT analysis of nanostructures, including nanoparticles, nanosheets, and nanowires, was the development of appropriate specimen preparation approaches, as these materials, unlike bulk materials, do not allow straightforward traditional protocols to prepare needle-shaped specimens (Felfer et al., 2015). Common workarounds include the deposition of nanoparticles on presharpened needles by electrophoresis (Tedsree et al., 2011), or the fixation of nanoparticles with a micromanipulator and subsequent coating on a support (Devaraj et al., 2015) followed by sharpening by focused ion beam (FIB) milling. Attachment on presharpened needles combined with a coating has also been proposed (Josten & Felfer, 2022). The deposition of a dense matrix material encapsulating the nanoparticles by atomic layer deposition (Larson et al., 2015) or metallic electrodeposition (Kim et al., 2018) enables the utilization of the commonly used specimen preparation using a dual beam scanning electron microscope (SEM)-FIB (Thompson et al., 2007). In the case of nanowires, their needle-like shape may even allow them to be analyzed without special specimen preparation in an atom probe with a local electrode (Perea et al., 2006; Du et al., 2013).

Despite the wide range of compositions available, and the increasing intensity of research on nanostructures, 2D materials such as MXenes have rarely been investigated using APT. Although graphene is occasionally used to coat biological or liquid APT specimens (Adineh et al., 2018; Qiu et al., 2020a, 2020b, 2020c), the analysis of graphene is only incidental. Previous studies have shown how APT can advance our understanding on the detailed composition of 2D materials, such as the incorporation of impurity elements during the wet chemical synthesis of 2D MoS_2 (Kim et al., 2020), or the influence of alkali elements from synthesis on the oxidation of $Ti_3C_2T_z$ MXenes (Krämer et al., 2024). In both cases, the nanosheets were embedded in a metallic matrix, but they are very difficult to localize for targeted sample preparation, and the small number of nanosheets in an average dataset limits the statistics.

Here, APT analysis is performed by taking advantage of the possibility to process MXenes into free-standing films, i.e. a macroscopic stack of nanosheets with the same orientation held together by weak intermolecular forces such as van der Waals forces or hydrogen bonds. APT specimens of a free-standing $Ti_3C_2T_z$ MXene film were prepared by FIB lift-out. Following sharpening, APT specimens were coated *in situ* by ion milling a Cr lamella as a sputter target (Woods et al., 2023), to mechanically stabilize the fragile specimens. In addition to enhanced yield, performance, and increased field-of-view (Schwarz et al., 2024), as well as the reduction of artifacts in the analysis of Li-containing materials (Singh et al., 2024), the presented workflow involving the *in situ* coating technique may also be a starting point for a simplified and straightforward APT analysis of 2D materials.

Materials and Methods

Synthesis of Ti_3AlC_2 MAX Phase

Ti_3AlC_2 MAX phase was synthesized by solid–liquid reaction. Briefly, TiC (99.5 %, Alfa Aesar), Ti (99.7 %, Strem), and Al (99.7 %, Strem) powders were ball milled at 1800 rpm for a duration of 5 min. The resulting powder mixture was cold pressed and then heat treated in a furnace at 1500 °C for a period of 120 min under a protective Ar environment. Finally, the sintered Ti_3AlC_2 MAX phase was ball milled at 1800 rpm for 5 min to a fine powder, ready for MXene synthesis.

Synthesis of $Ti_3C_2T_z$ MXenes

For $Ti_3C_2T_z$ MXene synthesis, 0.5 g LiF (99 %, Strem) was dissolved in 5 mL 10.2 mol L^{-1} concentrated HCl (32 %, Bio-Lab) in a high-density polyethylene vial, to prepare the etchant for selective etching of the Al layer from the previous sintered Ti_3AlC_2 MAX phase. Etching was done by slowly adding 0.5 g of the MAX phase powder to the solution under constant stirring with a magnetic stirrer at 45 °C for 24 h.

After etching, the complete solution was transferred to a 50 mL centrifuge tube and filled with deionized water (conductivity 0.055 μS cm^{-1}). The solution was shaken thoroughly and then centrifuged at 3500 rpm for a duration of 2 min. The supernatant was decanted, and the remaining sediment was replenished with deionized water, shaken and centrifuged again. Washing was repeated several times until the solution reached a near-neutral pH value, i.e. greater than 6. After washing, the tube containing the sediment was refilled with deionized water and the solution was sonicated in an ice bath for 60 min to prevent heating. To remove unetched residues of the MAX phase, the solution was centrifuged at 3500 rpm for 30 min and the black colloidal supernatant containing single layer MXenes was collected. Finally, the colloidal solution with a yield of about 7 g L^{-1} was stored at 5 °C.

Preparing Free-Standing $Ti_3C_2T_z$ MXene Film

The free-standing MXene film was prepared by vacuum filtration. 5 mL of the colloidal solution was poured into a vacuum filtration system using a Celgard® 3501 membrane. After filtration, the film was removed from the membrane. Figure 1 shows both the top (a) and the cross-sectional view (b) of the free-standing film, revealing the horizontal alignment of the nanosheets in the stack.

APT Specimen Preparation

Needle-shaped APT specimens were prepared using a dual beam SEM-FIB (Helios Nanolab 600, FEI) equipped with a Ga ion source and a Kleindiek micromanipulator. A first batch of specimens was prepared from the free-standing MXene film according to the lift-out and sharpening protocol introduced by Thompson et al. (2007), as illustrated in Figures 2a–2d. For a second batch of specimens, a tool with a horizontal needle that allows for free axial rotation (Cameca Instruments) was loaded into the chamber of the dual beam SEM-FIB. The workflow essentially followed the lift-out and sharpening

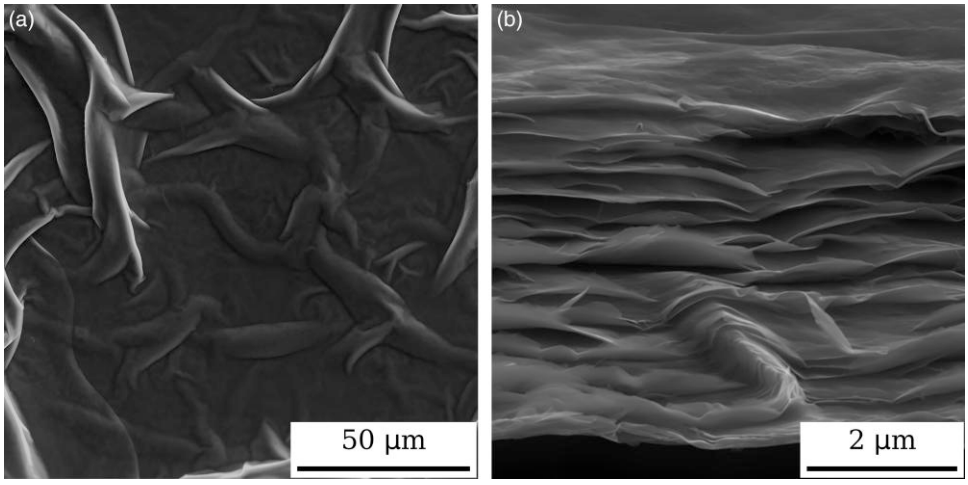

Fig. 1. (**a**) Top and (**b**) cross-sectional view of the free-standing $Ti_3C_2T_z$ MXene film.

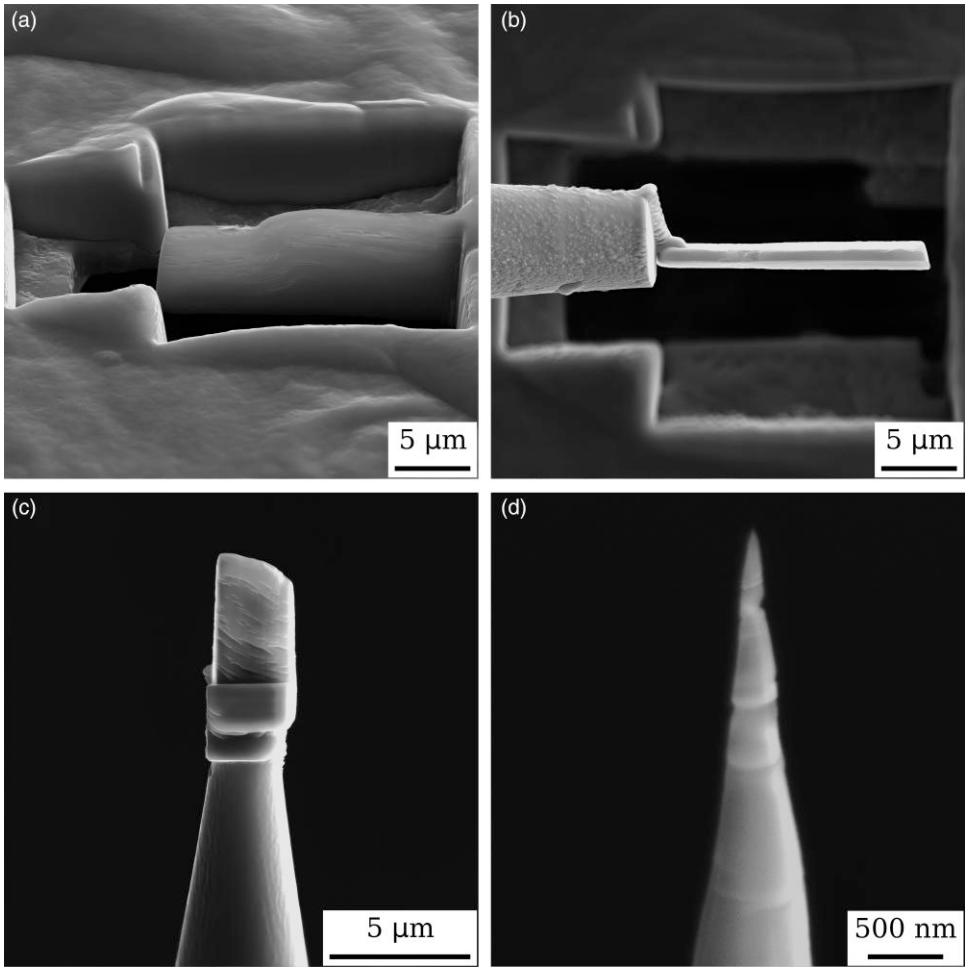

Fig. 2. APT specimen preparation of the free-standing $Ti_3C_2T_z$ MXene film following common lift-out and sharpening protocols. (**a**) Cross-sectional view of a lamella sliced out of the film using the Ga ion beam. (**b**) Lift-out of the lamella, which is attached to a micromanipulator by decomposing a gaseous Pt/C precursor from a gas-injection system. (**c**) Mounted lift-out on a commercial silicon support. (**d**) Final sharpened APT specimen after annular ion milling. The horizontal stacking orientation of the nanosheets is readily visible.

protocol described above, except that the lifted-out lamella was first attached from the micromanipulator onto the inserted needle. The chamber of the dual-beam instrument was vented, and the needle was manually rotated axially by 90°, thereby aligning the MXene nanosheets more favorably for APT analysis. After loading the tool with the needle back into the dual beam SEM-FIB, the lift-out was picked up again with the micromanipulator to continue with common

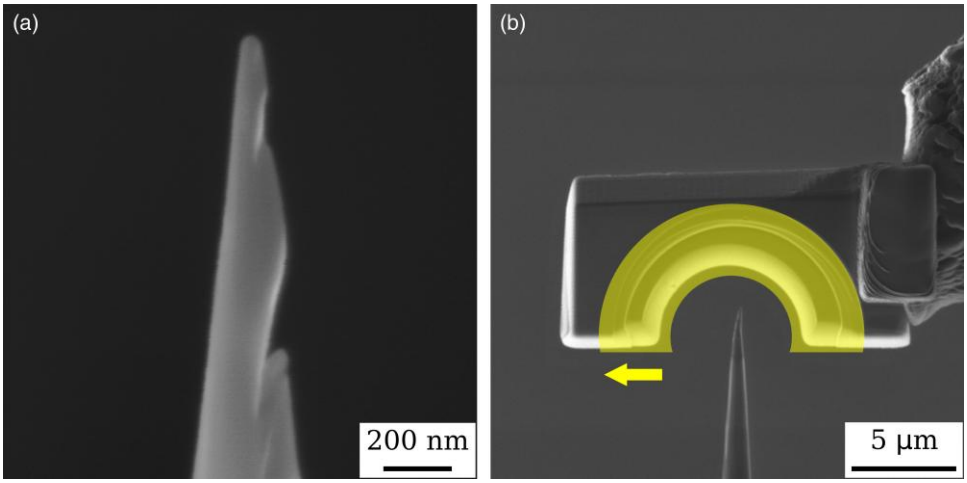

Fig. 3. Revised APT specimen preparation for the free-standing $Ti_3C_2T_z$ MXene film utilizing the *in situ* sputtering technique. (**a**) Uncoated APT specimen. The lift-out was rotated to orient the nanosheets along the specimen. (**b**) *In situ* coating procedure. The milling pattern is schematically shown in yellow.

specimen preparation workflow. Following annular ion milling, specimens such as in Figure 3a were then additionally coated with Cr (99.9 % purity) using an *in situ* sputtering technique described by Woods et al. (2023), building on previous reported works (Kölling & Vandervorst, 2009; Douglas et al., 2023), and as depicted in Figure 3b. More details on the complete coating workflow can be found in Schwarz et al. (2024). Sputtering parameters for the ion beam pattern were 30 kV and 48 pA for 20–30 s, repeated four times after rotating the specimen 90° each time to ensure a uniform coating. Cr as a coating material was chosen in first place for its well-known adhesion properties.

APT Characterization

APT analyses were performed using either a 5000XS (straight flight path) or a 5000XR (reflectron-fitted) local electrode atom probe (Cameca Instruments), operating in ultraviolet ($\lambda = 355$ nm) laser-pulsing mode. Parameters were set to a base temperature of 50 K, a laser pulse energy varied between 50 and 75 pJ, a laser pulsing rate of 125 kHz, and a target detection rate of 5–10 ions per 1000 pulses on average. Data reconstruction and analysis were done with AP Suite 6.3 by Cameca Instruments following the default voltage-based reconstruction algorithm.

Results and Discussion

Mechanical Instability and In Situ *Delithiation*

Initial attempts to analyze APT specimens of the free-standing MXene film, prepared as described in Figure 4, faced significant problems with the mechanical stability of the specimens, that may be inherent in the APT analysis of such materials. In this arrangement, the stacking orientation of the nanosheets is perpendicular to the main axis of the APT specimen, as visible in Figure 2d. Despite the intermolecular interactions between the MXenes nanosheets, they are not strong enough to withstand the high Maxwell stresses arising from the intense electrostatic field applied during the analysis (Rendulic & Müller, 1967; Moy et al., 2011). In addition, there may also be nanovoids between the nanosheets, as visible in the cross-sectional view of the free-standing film in Figure 1b, where intermolecular forces will be almost absent. This results in multiple small fractures, i.e. the partial mechanical failure of the specimen (Wilkes et al., 1972), as evidenced by drops in the base voltage curve in Figure 4a, which can be explained by a sudden increase in the detection rate due to the detection of several nanosheets breaking off from the specimen apex in very close succession. In almost all cases, measurements are limited to less than a million ions detected before the specimens fractures completely from the silicon support, so the success rate for these samples is rather low.

Li was normally only used in the wet chemical synthesis for exfoliation. However, here up to 90 at.% Li was measured in the analyzed specimens. In the reconstructed 3D atom map in Figure 4b, it was observed that at the beginning and then after each microfracture, Li field evaporates first before other species such as Ti are also detected. During APT analysis, the intense electrostatic field can cause preferential migration of Li atoms (Greiwe et al., 2014), also known as *in situ* delithiation (Pfeiffer et al., 2017), which is a known artifact in the analysis of Li-containing materials. Hot spots in the detector map in Figure 4c, localized preferentially on the side of the specimen directly illuminated by the laser, are another indicator for this phenomenon, since the temperature rise of the specimen due to the absorbed laser energy increases the mobility and thus the migration of the Li atoms (Kim et al., 2022). Considering the observed mechanical instability of the specimen, the *in situ* delithiation could possibly even favor it, since the sudden deintercalation of Li may weaken the intermolecular forces between the nanosheets.

In summary, it was not possible to perform a reliable APT analysis on specimens of the free-standing 2D material film prepared using the common FIB lift-out and sharpening protocols. On the one hand, the specimens lack mechanical stability, and on the other hand, preferential migration of Li atoms prevents detailed compositional analysis.

In Situ *Coating for Mechanical Stabilization*

In order to overcome both the mechanical instability and *in situ* delithiation issue that hinder successful APT analysis of the free-standing $Ti_3C_2T_z$ MXene film, specimens were prepared according to the workflow described in Figure 3. Coating of APT specimens resulted in enhanced yield for a wide range of materials (Kölling & Vandervorst, 2009; Larson et al., 2013;

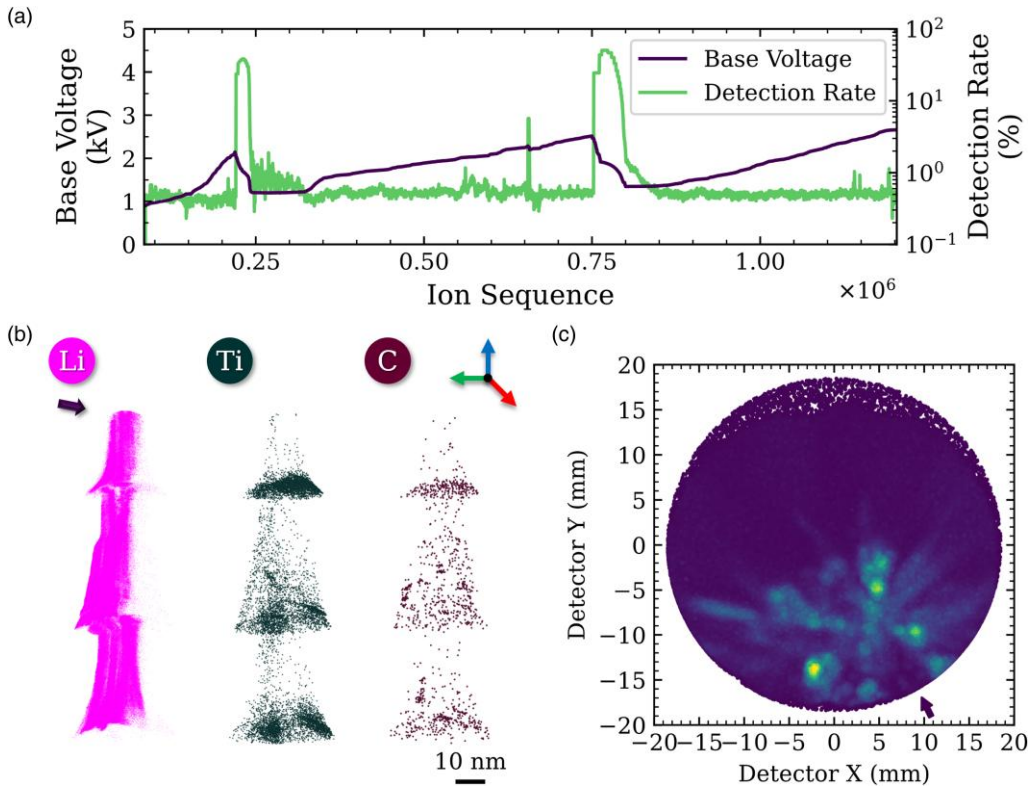

Fig. 4. Characteristic APT analysis of the free-standing MXene film prepared following common lift-out and sharpening protocols. (**a**) Base voltage and detection rate curve. (**b**) Reconstructed 3D atom maps. (**c**) Detector hit map. The direction of the laser beam is indicated by an arrow.

Schwarz et al., 2024), for example by smoothing out the roughness of the specimen surface, but also suppressed *in situ* delithiation in battery materials (Kim et al., 2022; Singh et al., 2024), or the piezoelectric effect in perovskite-structured materials (Kim et al., 2023) by shielding the electrostatic field. By sputtering a material onto the specimen, pores and nanovoids may also be filled, which helps to reduce varying magnification in the reconstruction due to ion trajectory aberrations as well as possible crack tips for premature fracture during analysis (Pfeiffer et al., 2015). Various methods have been proposed to eliminate pores in APT specimens, such as electron beam-induced deposition (Pfeiffer et al., 2015; Barroo et al., 2020), electrodeposition (El-Zoka et al., 2017; Mouton et al., 2017), liquid metal encapsulation (Kim et al., 2022), or resin impregnation (Zand et al., 2023). However, these potential solutions have all their own drawbacks, such as exposing the material to an electrochemical environment, heat, or high pressure, which could alter the chemistry or structure of the material. *In situ* coating, on the other hand, has the advantage that a variety of materials can be used as sputter targets (Schwarz et al., 2024), and it can even be performed at cryogenic temperatures (Woods et al., 2023), minimizing the potential impact on the chemistry and structure of the material.

After metallic coating using the *in situ* sputtering technique, more than half a dozen specimens of the free-standing MXene film were successfully analyzed by APT, as exemplified in Figure 5. As visible in the cross-section of the reconstructed 3D atom map in Figure 5a, the as-prepared free-standing MXene film specimen is well coated by Cr. In addition to Cr, the coating itself contains also O, which passivates the Cr during the sputtering process itself, and Ga from the ion source, as discussed in more detail by Schwarz et al. (2024). Some of the Cr coating also seems to have penetrated into the stacked material, oriented along the specimen, and filled nanovoids between the nanosheets, as highlighted in the 2D compositional contour plots in Figure 5c, thus mechanically stabilizing the specimen. The quality of the metallic coating determines whether the specimens can be analyzed in the atom probe.

Figure 5b provides a plot of the base voltage and the background level curve of these data, both metrics that indicate measurement stability. Except for small drops, the base voltage steadily and smoothly increases, indicating stable field evaporation conditions. The background is largely constant and below 10 ppm ns^{-1} on average. Previous studies have shown that a low and constant background level is essential for the detailed quantification of alkali elements such as Li (Santhanagopalan et al., 2015; Lu et al., 2017; Kim et al., 2022), which can be lost in the background from uncorrelated DC field evaporation due to their low expected evaporation field compared to the other elements composing the material (Tsong, 1978). In addition, the detector hit maps of the Cr coated samples in Figure 5d do not show characteristic hot spots, that would indicate a preferential migration of Li atoms. This confirms that the Cr coating prevents the *in situ* delithiation, as was suggested in previous studies (Singh et al., 2024). Normalized to 3 Ti atoms, a content of 0.41 Li was measured in the region of interest, encompassed by the dark green-cyan iso-compositional surface of 15 at.% Ti in Figure 5a, which is comparable to inductively coupled plasma mass spectrometry data for $Ti_3C_2T_z$ MXenes, where Li was also utilized in the synthesis for intercalation (Sharma et al., 2017).

Compared to previous work, where exfoliated $Ti_3C_2T_z$ MXenes were electrodeposited into Co (Krämer et al.,

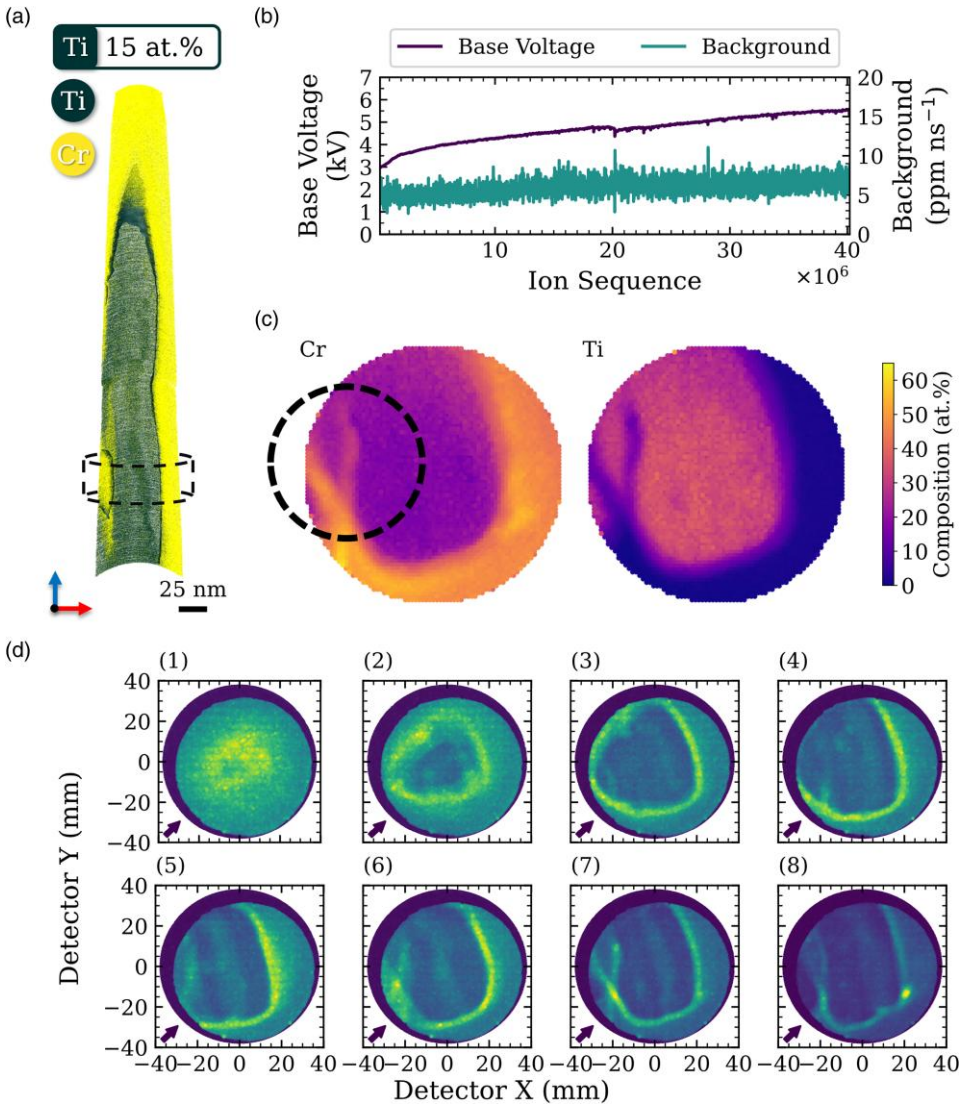

Fig. 5. Characteristic APT analysis of the free-standing MXene film prepared following the revised specimen preparation. (**a**) Cross section of the reconstructed 3D atom map. (**b**) Base voltage and background level curve. (**c**) 2D compositional contour plots of the extracted region of interest highlighted in (**a**). (**d**) History of the detector hit map during the measurement, starting at (1). The direction of the laser beam is indicated by an arrow.

2024), significantly larger volumes of the material of interest were measured. To illustrate the improvement, the detected Ti ion counts, including the contribution of decomposed molecular ions, from the APT data of the exfoliated MXenes from Krämer et al. (2024) and the free-standing MXenes films were compared. While less than 0.1 million Ti ions were detected in the dataset for the exfoliated MXenes embedded in Co, between 1.5 and 2 million Ti ions were collected in the free-standing MXene film in different measurements. All these values refer to data acquired on a 5000XR instrument with a detection efficiency of 52 %, as stated by Cameca Instruments. Notwithstanding the much simpler and time-saving specimen preparation workflow, the APT data obtained for the nanomaterial is significantly larger and therefore statistically more reliable.

Besides Cr, other materials may also be considered as sputter targets in the future. Although it has been shown that specimens can be easily coated with Cr using the *in situ* sputtering technique, it has some disadvantages for this particular case. During the sputtering process, the clean Cr layer is constantly passivated with an oxide layer (Schwarz et al., 2024), despite the vacuum inside the SEM-FIB. Since the coating also penetrates into the free-standing film specimen itself to fill nanovoids, the detailed determination of the oxygen content of the nanomaterial becomes nearly impossible. Therefore, Cr should be replaced as coating material by a more chemically inert metal in further studies, depending on the adhesion and the probability of peak overlap with the material of interest in the APT mass spectrum.

Conclusion

Despite the great interest in understanding the functional properties of nanomaterials by characterizing their detailed composition, 2D materials have rarely been studied using APT. Using $Ti_3C_2T_z$ MXenes as an example, the common SEM-FIB specimen preparation has been revised utilizing an *in situ* sputtering technique to facilitate the APT analysis of 2D materials. By processing the colloidal MXene solution into an additive-free free-standing film to enable a common

lift-out and sharpening procedure, and by coating the APT specimen, it was possible to acquire relatively large volumes of the 2D material with high data quality. The coating stabilizes the fragile specimen, but also prevents the *in situ* delithiation of Li, which was incorporated into the material during synthesis. As materials other than MXenes can also be processed into free-standing films (Dikin et al., 2007; Li et al., 2023), the presented workflow has the potential to be a starting point to study the detailed composition of 2D materials with APT.

Availability of Data and Materials

The data that support the findings of this study are available from the corresponding authors upon reasonable request.

Acknowledgment

The authors thank Uwe Tezins, Andreas Sturm, and Christian Broß for their support to the FIB and APT facilities at the Max Planck Institute for Sustainable Materials.

Financial Support

The authors are grateful for financial support from the German Research Foundation (DFG) through DIP Project No. 450800666.

Conflict of Interest

The authors declare no conflict of interest.

References

Adineh VR, Zheng C, Zhang Q, Marceau RKW, Liu B, Chen Y, Si KJ, Weyland M, Velkov T, Cheng W, Li J & Fu J (2018). Graphene-enhanced 3D chemical mapping of biological specimens at near-atomic resolution. *Adv Funct Mater* **28**(32), 1801439. https://doi.org/10.1002/adfm.201801439

Alhabeb M, Maleski K, Anasori B, Lelyukh P, Clark L, Sin S & Gogotsi Y (2017). Guidelines for synthesis and processing of two-dimensional titanium carbide ($Ti_3C_2T_x$ MXene). *Chem Mater* **29**(18), 7633–7644. https://doi.org/10.1021/acs.chemmater.7b02847

Anasori B & Naguib M, & Guest Editors (2023). Two-dimensional MXenes. *MRS Bull* **48**(3), 238–244. https://doi.org/10.1557/s43577-023-00500-z

Barroo C, Akey AJ & Bell DC (2020). Aggregated nanoparticles: Sample preparation and analysis by atom probe tomography. *Ultramicroscopy* **218**, 113082. https://doi.org/10.1016/j.ultramic.2020.113082

Chen H, Wen Y, Qi Y, Zhao Q, Qu L & Li C (2020). Pristine titanium carbide MXene films with environmentally stable conductivity and superior mechanical strength. *Adv Funct Mater* **30**(5), 1906996. https://doi.org/10.1002/adfm.201906996

De Geuser F & Gault B (2020). Metrology of small particles and solute clusters by atom probe tomography. *Acta Mater* **188**, 406–415. https://doi.org/10.1016/j.actamat.2020.02.023

Devaraj A, Gu M, Colby R, Yan P, Wang CM, Zheng JM, Xiao J, Genc A, Zhang JG, Belharouak I, Wang D, Amine K & Thevuthasan S (2015). Visualizing nanoscale 3D compositional fluctuation of lithium in advanced lithium-ion battery cathodes. *Nat Commun* **6**(1), 8014. https://doi.org/10.1038/ncomms9014

Dikin DA, Stankovich S, Zimney EJ, Piner RD, Dommett GHB, Evmenenko G, Nguyen ST & Ruoff RS (2007). Preparation and characterization of graphene oxide paper. *Nature* **448**(7152), 457–460. https://doi.org/10.1038/nature06016

Douglas JO, Conroy M, Giuliani F & Gault B (2023). In situ sputtering from the micromanipulator to enable cryogenic preparation of specimens for atom probe tomography by focused-ion beam. *Microsc Microanal* **29**(3), 1009–1017. https://doi.org/10.1093/micmic/ozad020

Du S, Burgess T, Loi ST, Gault B, Gao Q, Bao P, Li L, Cui X, Yeoh WK, Tan HH, Jagadish C, Ringer SP & Zheng R (2013). Full tip imaging in atom probe tomography. *Ultramicroscopy* **124**, 96–101. https://doi.org/10.1016/j.ultramic.2012.08.014

El-Zoka A, Langelier B, Botton G & Newman R (2017). Enhanced analysis of nanoporous gold by atom probe tomography. *Mater Charact* **128**, 269–277. https://doi.org/10.1016/j.matchar.2017.03.013

Felfer P, Li T, Eder K, Galinski H, Magyar A, Bell D, Smith G, Kruse N, Ringer S & Cairney J (2015). New approaches to nanoparticle sample fabrication for atom probe tomography. *Ultramicroscopy* **159**, 413–419. https://doi.org/10.1016/j.ultramic.2015.04.014

Gault B, Chiaramonti A, Cojocaru-Mirédin O, Stender P, Dubosq R, Freysoldt C, Makineni SK, Li T, Moody M & Cairney JM (2021). Atom probe tomography. *Nat Rev Methods Primers* **1**(1), 51. https://doi.org/10.1038/s43586-021-00047-w

Ghidiu M, Lukatskaya MR, Zhao M-Q, Gogotsi Y & Barsoum MW (2014). Conductive two-dimensional titanium carbide 'clay' with high volumetric capacitance. *Nature* **516**(7529), 78–81. https://doi.org/10.1038/nature13970

Greiwe G-H, Balogh Z & Schmitz G (2014). Atom probe tomography of lithium-doped network glasses. *Ultramicroscopy* **141**, 51–55. https://doi.org/10.1016/j.ultramic.2014.03.007

Josten JP & Felfer PJ (2022). Atom probe analysis of nanoparticles through pick and coat sample preparation. *Microsc Microanal* **28**(4), 1188–1197. https://doi.org/10.1017/S1431927621000465

Kim S-H, Antonov S, Zhou X, Stephenson LT, Jung C, El-Zoka AA, Schreiber DK, Conroy M & Gault B (2022). Atom probe analysis of electrode materials for Li-ion batteries: Challenges and ways forward. *J Mater Chem A* **10**(9), 4926–4935. https://doi.org/10.1039/D1TA10050E

Kim S-H, El-Zoka AA & Gault B (2022). A liquid metal encapsulation for analyzing porous nanomaterials by atom probe tomography. *Microsc Microanal* **28**(4), 1198–1206. https://doi.org/10.1017/S1431927621012964

Kim S-H, Kang PW, Park OO, Seol J-B, Ahn J-P, Lee JY & Choi P-P (2018). A new method for mapping the three-dimensional atomic distribution within nanoparticles by atom probe tomography (APT). *Ultramicroscopy* **190**, 30–38. https://doi.org/10.1016/j.ultramic.2018.04.005

Kim S-H, Lim J, Sahu R, Kasian O, Stephenson LT, Scheu C & Gault B (2020). Direct imaging of dopant and impurity distributions in 2D MoS_2. *Adv Mater* **32**(8), 1907235. https://doi.org/10.1002/adma.201907235

Kim S-H, Shin K, Zhou X, Jung C, Kim HY, Pedrazzini S, Conroy M, Henkelman G & Gault B (2023). Atom probe analysis of $BaTiO_3$ enabled by metallic shielding. *Scr Mater* **229**, 115370. https://doi.org/10.1016/j.scriptamat.2023.115370

Kölling S & Vandervorst W (2009). Failure mechanisms of silicon-based atom-probe tips. *Ultramicroscopy* **109**(5), 486–491. https://doi.org/10.1016/j.ultramic.2008.11.013

Krämer M, Favelukis B, El-Zoka AA, Sokol M, Rosen BA, Eliaz N, Kim S-H & Gault B (2024). Near-atomic-scale perspective on the oxidation of $Ti_3C_2T_x$ MXenes: Insights from atom probe tomography. *Adv Mater* **36**(3), 2305183. https://doi.org/10.1002/adma.202305183

Lan C, Zhou Z, Wei R & Ho JC (2019). Two-dimensional perovskite materials: From synthesis to energy-related applications. *Mater Today Energy* **11**, 61–82. https://doi.org/10.1016/j.mtener.2018.10.008

Larson D, Giddings A, Wu Y, Verheijen M, Prosa T, Roozeboom F, Rice K, Kessels W, Geiser B & Kelly T (2015). Encapsulation method for atom probe tomography analysis of nanoparticles. *Ultramicroscopy* **159**, 420–426. https://doi.org/10.1016/j.ultramic.2015.02.014

Larson D, Prosa T, Bunton J, Olson D, Lawrence D, Oltman E, Strennin S & Kelly T (2013). Improved mass resolving power and yield in

atom probe tomography. *Microsc Microanal* **19**(S2), 994–995. https://doi.org/10.1017/S143192761300696X

Li T, Devaraj A & Kruse N (2022). Atomic-scale characterization of (electro-)catalysts and battery materials by atom probe tomography. *Cell Rep* **3**(12), 101188. https://doi.org/10.1016/j.xcrp.2022.101188

Li X & Lu K (2017). Playing with defects in metals. *Nat Mater* **16**(7), 700–701. https://doi.org/10.1038/nmat4929

Li Z, Sami I, Yang J, Li J, Kumar RV & Chhowalla M (2023). Lithiated metallic molybdenum disulfide nanosheets for high-performance lithium–sulfur batteries. *Nat Energy* **8**(1), 84–93. https://doi.org/10.1038/s41560-022-01175-7

Lim KRG, Shekhirev M, Wyatt BC, Anasori B, Gogotsi Y & Seh ZW (2022). Fundamentals of MXene synthesis. *Nat Synth* **1**(8), 601–614. https://doi.org/10.1038/s44160-022-00104-6

Lipatov A, Alhabeb M, Lukatskaya MR, Boson A, Gogotsi Y & Sinitskii A (2016). Effect of synthesis on quality, electronic properties and environmental stability of individual monolayer Ti_3C_2 MXene flakes. *Adv Electron Mater* **2**(12), 1600255. https://doi.org/10.1002/aelm.201600255

Lu X, Schreiber DK, Neeway JJ, Ryan JV & Du J (2017). Effects of optical dopants and laser wavelength on atom probe tomography analyses of borosilicate glasses. *J Am Ceramic Soc* **100**(10), 4801–4815. https://doi.org/10.1111/jace.2017.100.issue-10

Lukatskaya MR, Mashtalir O, Ren CE, Dall'Agnese Y, Rozier P, Taberna PL, Naguib M, Simon P, Barsoum MW & Gogotsi Y (2013). Cation intercalation and high volumetric capacitance of two-dimensional titanium carbide. *Science* **341**(6153), 1502–1505. https://doi.org/10.1126/science.1241488

Mannix AJ, Kiraly B, Hersam MC & Guisinger NP (2017). Synthesis and chemistry of elemental 2D materials. *Nat Rev Chem* **1**(2), 0014. https://doi.org/10.1038/s41570-016-0014

Manzeli S, Ovchinnikov D, Pasquier D, Yazyev OV & Kis A (2017). 2D transition metal dichalcogenides. *Nat Rev Mater* **2**(8), 17033. https://doi.org/10.1038/natrevmats.2017.33

Mouton I, Printemps T, Grenier A, Gambacorti N, Pinna E, Tiddia M, Vacca A & Mula G (2017). Toward an accurate quantification in atom probe tomography reconstruction by correlative electron tomography approach on nanoporous materials. *Ultramicroscopy* **182**, 112–117. https://doi.org/10.1016/j.ultramic.2017.06.007

Moy CK, Ranzi G, Petersen TC & Ringer SP (2011). Macroscopic electrical field distribution and field-induced surface stresses of needle-shaped field emitters. *Ultramicroscopy* **111**(6), 397–404. https://doi.org/10.1016/j.ultramic.2011.01.024

Naguib M, Kurtoglu M, Presser V, Lu J, Niu J, Heon M, Hultman L, Gogotsi Y & Barsoum MW (2011). Two-dimensional nanocrystals produced by exfoliation of Ti_3AlC_2. *Adv Mater* **23**(37), 4248–4253. https://doi.org/10.1002/adma.v23.37

Nicolosi V, Chhowalla M, Kanatzidis MG, Strano MS & Coleman JN (2013). Liquid exfoliation of layered materials. *Science* **340**(6139), 1226419. https://doi.org/10.1126/science.1226419

Novoselov KS, Geim AK, Morozov SV, Jiang D, Zhang Y, Dubonos SV, Grigorieva IV & Firsov AA (2004). Electric field effect in atomically thin carbon films. *Science* **306**(5696), 666–669. https://doi.org/10.1126/science.1102896

Perea DE, Allen JE, May SJ, Wessels BW, Seidman DN & Lauhon LJ (2006). Three-dimensional nanoscale composition mapping of semiconductor nanowires. *Nano Lett* **6**(2), 181–185. https://doi.org/10.1021/nl051602p

Pfeiffer B, Erichsen T, Epler E, Volkert CA, Trompenaars P & Nowak C (2015). Characterization of nanoporous materials with atom probe tomography. *Microsc Microanal* **21**(3), 557–563. https://doi.org/10.1017/S1431927615000501

Pfeiffer B, Maier J, Arlt J & Nowak C (2017). In situ atom probe deintercalation of lithium-manganese-oxide. *Microsc Microanal* **23**(2), 314–320. https://doi.org/10.1017/S1431927616012691

Qiu S, Garg V, Zhang S, Chen Y, Li J, Taylor A, Marceau RK & Fu J (2020). Graphene encapsulation enabled high-throughput atom probe tomography of liquid specimens. *Ultramicroscopy* **216**, 113036. https://doi.org/10.1016/j.ultramic.2020.113036

Qiu S, Zheng C, Garg V, Chen Y, Gervinskas G, Li J, Dunstone MA, Marceau RKW & Fu J (2020). Three-dimensional chemical mapping of a single protein in the hydrated state with atom probe tomography. *Anal Chem* **92**(7), 5168–5177. https://doi.org/10.1021/acs.analchem.9b05668

Qiu S, Zheng C, Zhou Q, Dong D, Shi Q, Garg V, Cheng W, Marceau RK, Sha G & Fu J (2020). Direct imaging of liquid–nanoparticle interfaces with atom probe tomography. *J Phys Chem C* **124**(35), 19389–19395. https://doi.org/10.1021/acs.jpcc.0c05504

Rendulic KD & Müller EW (1967). Elastic deformation of field-ion-microscope tips. *J Appl Phys* **38**(5), 2070–2072. https://doi.org/10.1063/1.1709831

Sang X, Xie Y, Lin M-W, Alhabeb M, Aken KLVan, Gogotsi Y, Kent PRC, Xiao K & Unocic RR (2016). Atomic defects in monolayer titanium carbide ($Ti_3C_2T_x$) MXene. *ACS Nano* **10**(10), 9193–9200. https://doi.org/10.1021/acsnano.6b05240

Santhanagopalan D, Schreiber DK, Perea DE, Martens RL, Janssen Y, Khalifah P & Meng YS (2015). Effects of laser energy and wavelength on the analysis of $LiFePO_4$ using laser assisted atom probe tomography. *Ultramicroscopy* **148**, 57–66. https://doi.org/10.1016/j.ultramic.2014.09.004

Schwarz TM, Woods E, Singh MP, Chen X, Jung C, Aota LS, Jang K, Krämer M, Kim S-H & McCarroll I (2024). In situ metallic coating of atom probe specimen for enhanced yield, performance, and increased field-of-view. *Microsc Microanal*, ozae006. https://doi.org/10.1093/mam/ozae006

Sharma G, Muthuswamy E, Naguib M, Gogotsi Y, Navrotsky A & Wu D (2017). Calorimetric study of alkali metal ion (K^+, Na^+, Li^+) exchange in a clay-like MXene. *J Phys Chem C* **121**(28), 15145–15153. https://doi.org/10.1021/acs.jpcc.7b02419

Shekhirev M, Busa J, Shuck CE, Torres A, Bagheri S, Sinitskii A & Gogotsi Y (2022). Ultralarge flakes of $Ti_3C_2T_x$ MXene via soft delamination. *ACS Nano* **16**(9), 13695–13703. https://doi.org/10.1021/acsnano.2c04506

Shekhirev M, Shuck CE, Sarycheva A & Gogotsi Y (2021). Characterization of MXenes at every step, from their precursors to single flakes and assembled films. *Prog Mater Sci* **120**, 100757. https://doi.org/10.1016/j.pmatsci.2020.100757

Shuck CE (2023). MXenes are materials, not chemicals: Synthesis factors that influence MXene properties. *MRS Commun* **13**(6), 957–970. https://doi.org/10.1557/s43579-023-00442-2

Shuck CE, Sarycheva A, Anayee M, Levitt A, Zhu Y, Uzun S, Balitskiy V, Zahorodna V, Gogotsi O & Gogotsi Y (2020). Scalable synthesis of $Ti_3C_2T_x$ MXene. *Adv Eng Mater* **22**(3), 1901241. https://doi.org/10.1002/adem.201901241

Singh MP, Woods EV, Kim S-H, Jung C, Aota LS & Gault B (2024). Facilitating the systematic nanoscale study of battery materials by atom probe tomography through in-situ metal coating. *Batter Supercaps* **7**(2), e202300403. https://doi.org/10.1002/batt.202300403

Tedsree K, Li T, Jones S, Chan CWA, Yu KMK, Bagot PAJ, Marquis EA, Smith GDW & Tsang SCE (2011). Hydrogen production from formic acid decomposition at room temperature using a Ag–Pd core–shell nanocatalyst. *Nat Nanotechnol* **6**(5), 302–307. https://doi.org/10.1038/nnano.2011.42

Thakur A, Chandran BS N, Davidson K, Bedford A, Fang H, Im Y, Kanduri V, Wyatt BC, Nemani SK & Poliukhova V (2023). Step-by-step guide for synthesis and delamination of $Ti_3C_2T_x$ MXene. *Small Methods* **7**(8), 2300030. https://doi.org/10.1002/smtd.202300030

Thompson K, Lawrence D, Larson D, Olson J, Kelly T & Gorman B (2007). In situ site-specific specimen preparation for atom probe tomography. *Ultramicroscopy* **107**(2-3), 131–139. https://doi.org/10.1016/j.ultramic.2006.06.008

Tsong T (1978). Field ion image formation. *Surf Sci* **70**(1), 211–233. https://doi.org/10.1016/0039-6028(78)90410-7

VahidMohammadi A, Rosen J & Gogotsi Y (2021). The world of two-dimensional carbides and nitrides (MXenes). *Science* **372**(6547), eabf1581. https://doi.org/10.1126/science.abf1581

Wilkes TJ, Titchmarsh JM, Smith GDW, Smith DA, Morris RF, Johnston S, Godfrey TJ & Birdseye P (1972). The fracture of field-ion microscope specimens. *J Phys D Appl Phys* **5**(12), 2226–2230. https://doi.org/10.1088/0022-3727/5/12/312

Woods EV, Singh MP, Kim S-H, Schwarz TM, Douglas JO, El-Zoka AA, Giulani F & Gault B (2023). A versatile and reproducible cryo-sample preparation methodology for atom probe studies. *Microsc Microanal* **29**(6), 1992–2003. https://doi.org/10.1093/micmic/ozad120

Zand F, Hangx SJT, Spiers CJ, van den Brink PJ, Burns J, Boebinger MG, Poplawsky JD, Monai M & Weckhuysen BM (2023). Elucidating the structure and composition of individual bimetallic nanoparticles in supported catalysts by atom probe tomography. *J Am Chem Soc* **145**(31), 17299–17308. https://doi.org/10.1021/jacs.3c04474

Zhang J, Kong N, Uzun S, Levitt A, Seyedin S, Lynch PA, Qin S, Han M, Yang W & Liu J (2020). Scalable manufacturing of free-standing, strong $Ti_3C_2T_x$ MXene films with outstanding conductivity. *Adv Mater* **32**(23), 2001093. https://doi.org/10.1002/adma.202001093

Zhang C, McKeon L, Kremer MP, Park S-H, Ronan O, Seral-Ascaso A, Barwich S, Coileáin CÓ, McEvoy N, Nerl HC, Anasori B, Coleman JN, Gogotsi Y & Nicolosi V (2019). Additive-free MXene inks and direct printing of micro-supercapacitors. *Nat Commun* **10**(1), 1795. https://doi.org/10.1038/s41467-019-09398-1